EUROPEAN ORGANIZATION FOR NUCLEAR RESEARCH

L3 Note 2518
March 8, 2000

Preliminary Results on Single W Boson Production at 192 GeV $\leq \sqrt{s} \leq$ 202 GeV

L3 Collaboration

Abstract

Single W boson production in electron-positron collisions is analysed with the L3 detector at LEP. The data sample collected at a centre-of-mass energies of $\sqrt{s}$ = 192 GeV, 196 GeV, 200 GeV and 202 GeV corresponds to an integrated luminosity of $233.3\,\mathrm{pb}^{-1}$. Events with a single energetic lepton or two hadronic jets visible in the detector are selected. The total cross-sections are measured and found to be consistent with the Standard Model expectation. Including our single W boson results obtained at lower $\sqrt{s}$ the WWγ gauge couplings κ_γ and λ_γ are determined to be $\kappa_\gamma = +1.10^{+0.10}_{-0.11} \pm 0.08$ and $\lambda_\gamma = -0.10^{+0.41}_{-0.22} \pm 0.11$. These results are preliminary.

Submitted to *2000 Winter Conferences*

1 Introduction

Precise measurements of trilinear gauge boson couplings constitute a crucial test of the Standard Model of electroweak interactions [1]. The studies of the single W production at LEP [1)]

$$\mathrm{e^+e^-} \rightarrow \mathrm{e^+}\nu_\mathrm{e}\mathrm{W^-} \tag{1}$$

by the LEP experiments [2–4] demonstrated that this process provides one of the best experimental grounds for precision measurements of the electromagnetic gauge couplings of the W boson. The cross-section of process (1) depends only on the κ_γ and λ_γ gauge coupling parameters [5]. Despite the low cross section of about 0.5 pb this process allows for a clean test of the WWγ vertex. Any deviation from the coupling values $\kappa_\gamma = 1$ and $\lambda_\gamma = 0$ predicted by the Standard Model would indicate that the W boson has an internal structure.

A specific feature of this reaction is a final state positron (electron) produced at very low polar angle and therefore not detected. Thus the signature of this process is a single energetic lepton, if the W boson decays into lepton and neutrino, or two hadronic jets and large transverse momentum imbalance in case of hadronic W decay.

In this article we report on the measurement of the cross section of single W boson production at the centre-of-mass energies between 192 GeV and 202 GeV. Including our results on single W boson production obtained at lower $\sqrt{s}$, we derive substantially more precise results on the gauge couplings κ_γ and λ_γ.

2 Data and Monte Carlo Samples

The data were collected by the L3 detector at LEP in 1999. The integrated luminosity is 233.3 pb^{-1} collected at four different energy points, $\sqrt{s} = 192$ GeV, 196 GeV, 200 GeV and 202 GeV. For signal studies samples of $\mathrm{e^+e^-} \rightarrow \mathrm{e^+}\nu_\mathrm{e}\mathrm{f\,\bar{f}'}$ events are generated using both the GRC4F [6] and the EXCALIBUR [7] Monte Carlo generators. For the background studies the following Monte Carlo programs are used: KORALZ [8] ($\mathrm{e^+e^-} \rightarrow \mu^+\mu^-(\gamma)$, $\tau^+\tau^-(\gamma)$), KORALW [9] ($\mathrm{e^+e^-} \rightarrow \mathrm{W^+W^-} \rightarrow \mathrm{f\,\bar{f}'f\,\bar{f}'}$), TEEGG [10] ($\mathrm{e^+e^-} \rightarrow \mathrm{e^+e^-}\gamma$), BHAGENE3 [11] and BHWIDE [12] ($\mathrm{e^+e^-} \rightarrow \mathrm{e^+e^-}(\gamma)$), PYTHIA [13] ($\mathrm{e^+e^-} \rightarrow \mathrm{q\,\bar{q}}(\gamma)$), KK [14] ($\mathrm{e^+e^-} \rightarrow \mathrm{f\,\bar{f}}(\gamma)$), PYTHIA and PHOJET [15] ($\mathrm{e^+e^-} \rightarrow \mathrm{e^+e^-e^+e^-}$, $\mathrm{e^+e^-}\mu^+\mu^-$, $\mathrm{e^+e^-}\tau^+\tau^-$, $\mathrm{e^+e^-q\,\bar{q}}$), and GRC4F and EXCALIBUR ($\mathrm{e^+e^-} \rightarrow \mathrm{f\,\bar{f}'f\,\bar{f}'}$).

The Monte Carlo events are simulated in the L3 detector using the GEANT 3.15 program [16], which takes into account the effects of energy loss, multiple scattering and showering in the detector. The GHEISHA program [17] is used to simulate hadronic interactions in the detector.

3 Analysis

The signal definition used here is the same as used before [2,3].The signal is defined as $\mathrm{e^+e^-} \rightarrow \mathrm{e^+}\nu_\mathrm{e}\,\mathrm{f\,\bar{f}'}$ events that satisfy the following phase space requirements:

$$\begin{aligned} |\cos\theta_{\mathrm{e^+}}| &> 0.997 \\ \min(E_\mathrm{f}, E_{\mathrm{\bar{f}'}}) &> 15 \text{ GeV} \\ |\cos\theta_{\mathrm{e^-}}| &< 0.75, \quad \text{for } \mathrm{e^+}\nu_\mathrm{e}\mathrm{e^-}\bar{\nu}_\mathrm{e} \text{ events only} \end{aligned} \tag{2}$$

[1)] The charge conjugate reactions are understood to be included throughout the paper.

where θ_{e^+} (θ_{e^-}) is the polar angle of the outgoing positron (electron), and E_{f} and $E_{\bar{\mathrm{f}}'}$ are the fermion energies. The final states $\mathrm{e^+e^-} \rightarrow \mathrm{e^+}\nu_{\mathrm{e}}\,\mathrm{f}\,\bar{\mathrm{f}}'$ that do not satisfy these conditions are considered as background; they consist mostly of the reaction $\mathrm{e^+e^-} \rightarrow \mathrm{W^+W^-}$. In the case of the $\mathrm{e^+}\nu_{\mathrm{e}}\,\mathrm{e^-}\bar{\nu}_{\mathrm{e}}$ final state the additional angular cut reduces contributions from processes where the $\nu_{\mathrm{e}}\bar{\nu}_{\mathrm{e}}$ pair originates from the decay of a Z boson.

Inside the phase space region (2) single W production (process 1) dominates since it peaks strongly at $|\cos\theta_{\mathrm{e^+}}| \sim 1$. On average it accounts for 90% of all events in this region, the remaining 10% being mostly non-resonant final states. The purity depends slightly on the flavour of the $\mathrm{f}\,\bar{\mathrm{f}}'$ pair from $\mathrm{W^-}$ decays and the centre-of-mass energy. For the $\mathrm{e^+}\nu_{\mathrm{e}}\,\mathrm{e^-}\bar{\nu}_{\mathrm{e}}$ final states the purity is lower than for other signal final states, it amounts to 75%.

All decay modes of the W boson are considered, leading to the following experimental signatures: events with single energetic electrons, muons and taus and events with two hadronic jets and large transverse momentum imbalance.

3.1 Hadronic Final States

The selection of candidates for the hadronic decay $\mathrm{W^-} \rightarrow \mathrm{q}\,\bar{\mathrm{q}}'$ of single W boson production, $\mathrm{e^+e^-} \rightarrow \mathrm{e^+}\nu_{\mathrm{e}}\mathrm{W^-}$, is based on the following requirements: two acoplanar hadronic jets, no leptons, and large transverse momentum imbalance.

High multiplicity hadronic events with at least six charged tracks are selected with large energy deposition in the electromagnetic calorimeter, $E_{\mathrm{ecal}} > 15$ GeV, and large total visible energy, $0.3 < E_{\mathrm{vis}}/\sqrt{s} < 0.8$. The transverse energy of the event is required to be greater than $E_{\perp}/E_{\mathrm{vis}} > 0.1$. All energy clusters in the event are combined to form two hadronic jets using the DURHAM algorithm [18]. The invariant mass of the two jets must be in the range 40 GeV $< M_{\mathrm{vis}} <$ 120 GeV. The energy in the forward luminosity calorimeters is required to be smaller than 60 GeV. These cuts reduce contributions from the purely leptonic final states $\mathrm{e^+e^-} \rightarrow \mathrm{e^+e^-}(\gamma)$, $\mu^+\mu^-(\gamma)$, $\tau^+\tau^-(\gamma)$ and two-photon interactions $\mathrm{e^+e^-} \rightarrow \mathrm{e^+e^-q\bar{q}}$ while keeping a significant fraction of hadronic events from the processes $\mathrm{e^+e^-} \rightarrow \mathrm{Z}(\gamma)$, $\mathrm{e^+e^-} \rightarrow \mathrm{W^+W^-}$ and $\mathrm{e^+e^-} \rightarrow \mathrm{ZZ}$.

To reject events from the two-fermion production process $\mathrm{e^+e^-} \rightarrow \mathrm{q\bar{q}}(\gamma)$ the transverse missing momentum is required to exceed 14 GeV. The angle between the missing momentum vector and the beam axis is restricted to $|\cos\theta_{\mathrm{mis}}| < 0.94$. In addition, the acoplanarity between the two jets must be larger than 10°. Additionally, the stereo angle between the two jets and the beam axis is required to be less than 5.5 srad.

Events containing identified electrons or photons with energy greater than 20 GeV or muons with energy greater than 15 GeV (30 GeV for MIPs) are rejected, in order to suppress the remaining background from $\mathrm{e^+e^-} \rightarrow \mathrm{W^+W^-}$ events where one of the W bosons decays into leptons. Three jets are formed for every remaining event using the DURHAM algorithm. The stereo angle, Ω, defined by the directions of these jets is required to be smaller than 5.0 srad. This criterion removes part of the remaining $\tau^+\nu_\tau\,\mathrm{q}\,\bar{\mathrm{q}}'$ final states with the τ lepton decaying hadronically. Moreover, candidates for τ-jets are separated from hadronic jets using a neural network. The following variables of a jet are fed into the network to identify the best candidate for a narrow τ-jet: cluster and track multiplicity, opening angle, mass, momentum and angular distance to the next jet. Events with a neural network output greater than 0.8 for the best τ-candidate are rejected. This improves the purity of the signal by approximately 4% to be compared to an efficiency loss of 1%.

From 189 GeV centre-of-mass energy onwards, the production of two on-mass-shell Z bosons is a source of a considerable background. A Z$\rightarrow \nu\bar{\nu}$ decay of one Z accompanied by a hadronic decay of the other Z leads to event signatures close to that of the signal process (1). To suppress this background, we make use of the fact, that the Z bosons produced in pairs are close to the kinematic threshold and therefore have low momenta and their decay products larger opening angles. A ZZ-probability is constructed using the velocity of the detected hadronic system, its invariant mass and its opening angle, the missing momentum and the reconstructed neutrino energy assuming the single W kinematics. The ZZ-probability is asked to be less than 0.96.

A total of 241 events is observed in data and is found to be consistent with the Standard Model predictions at all centre-of-mass energies. The contributions from the different processes at each centre-of-mass energy are listed in table 1. The signal efficiency is determined to be between 47.4% and 51.5% depending on the centre-of-mass energy.

In order to differentiate further between the signal and the WW background, a discriminant variable NN_{out} is constructed using a neural network approach. Nine event variables are combined using a feed-forward neural network [19], with one hidden layer and one output node. The input to the neural net includes three classes: global variables including the sphericity of the event, the velocity of the detected hadronic system, β, calculated as ratio of the missing momentum and the visible energy, $\beta = P_{\mathrm{mis}}/E_{\mathrm{vis}}$, and the event invariant mass; variables according to a 2-jet topology as the sum of masses of the two jets, the broadness of the first jet given by the ratio of its mass and energy and the reconstructed energy of the neutrino assuming single W kinematics; furthermore variables assuming a 3-jet topology as the stereo angle Ω, the distance scale parameter y_{34} of the JADE algorithm [20] for which the number of jets in the event changes from three to four and the minimal opening angle between two jets. As an example, the distribution of stereo angle Ω for the selected events is shown in Figure 1. The use of the neural network permits to increase the signal fraction in the selected sample for large neural network output values, as shown in Figure 2.

The cross-section of the process (1) for hadronic decays of the W boson is determined by a binned log-likelihood fit to the neural network output distribution, assuming Poisson statistics. The background contributions are kept fixed to the corresponding Standard Model Monte Carlo predictions. The fitted cross-section of the hadron channel for each energy point is listed in the following table and compared to the theoretical predictions calculated using EXCALIBUR and GRC4F, respectively.

$\sqrt{s}$ [GeV]	$\sigma_{\mathrm{qq}} \pm$ (stat.) $\pm$ (syst.) [pb]	$\sigma_{\mathrm{qq}}^{\mathrm{Ex}}$ [pb]	$\sigma_{\mathrm{qq}}^{\mathrm{Gr}}$ [pb]
192	$0.67 \ {}^{+0.35}_{-0.29} \ \pm 0.05$	0.398	0.406
196	$0.52 \ {}^{+0.19}_{-0.17} \ \pm 0.04$	0.439	0.435
200	$0.27 \ {}^{+0.18}_{-0.16} \ \pm 0.02$	0.461	0.465
202	$0.86 \ {}^{+0.32}_{-0.28} \ \pm 0.06$	0.474	0.480

As a cross-check, a fit of the WW cross-section, keeping the single W contribution fixed to the EXCALIBUR Monte Carlo prediction, shows reasonable agreement with the Standard Model expectation for WW production as predicted by KORALW.

The theoretical predictions presented in this note are calculated with an accuracy of approximately 0.2% - 1.0%. The current overall theoretical uncertainty on the single W cross section is of the order of 5%.

3.2 Leptonic Final States

A distinct feature of the process $e^+e^- \rightarrow e^+\nu_e W^-$, $W^- \rightarrow \ell^-\bar{\nu}_\ell$ is a high energy lepton from W decay with no other significant activity in the detector.

Events with one charged lepton identified either as electron, muon or hadronic τ-jet are selected. The lepton identification is based on the energy distribution in the electromagnetic and hadron calorimeters with respect to the trajectory of charged tracks. Events containing well measured tracks that do not belong to the lepton are rejected. The total energy, $E_{\rm tot}$, is calculated as the sum of the lepton energy, E_ℓ, and the energies of all neutral clusters in the event. The ratio $E_\ell/E_{\rm tot}$ for preselected events is required to exceed 0.93. In addition to this selection criterion, several other cuts are applied to suppress background from two fermion production $e^+e^- \rightarrow \ell^+\ell^-(\gamma)$: The acoplanarity between the lepton candidate and any track or calorimetric object that could be assigned to a second particle is required to be greater than 40°. Furthermore, the visible mass of all energy clusters is restricted by $M_{\rm vis}/\sqrt{s} < 0.1$.

Several selection criteria are imposed on the recoil side. Within the 30° azimuthal angle sector along the missing energy direction $\phi_{\rm mis}$, no significant activity is allowed, i.e. no vertex or muon chamber signal; the energy in the electromagnetic and the hadronic calorimeter should not exceed 200 MeV and 700 MeV, respectively; no scintillator signal in time ($\Delta t < 5\,$ns) with the beam-crossing. The energy in the forward-backward luminosity calorimeters, $E_{\rm FB}$, must be below 70 GeV.

3.2.1 Single Electron Final States

For the single electron final states, the electron energy must exceed 20 GeV and the polar angle is required to be $|\cos\theta_e| < 0.7$. This requirement reduces the contribution from Bhabha and Compton scattering and from the process $e^+e^- \rightarrow e^+e^-\nu\bar{\nu}$ where the e^+e^- pair originates from a low-mass virtual photon. The $e^+e^- \rightarrow e^+e^-(\gamma)$ events constitute the dominant contribution to the selected sample whose different configurations are described using the BHAGENE3, BHWIDE and TEEGG Monte Carlo generators. The requirements $E_e/E_{\rm tot} > 0.93$ and $E_{\rm FB} < 60$ GeV reduce significantly the contribution from $e^+e^- \rightarrow e^+e^-(\gamma)$. Photo-conversion in the process $e^+e^- \rightarrow \nu\bar{\nu}\gamma$ might fake a single electron. Since configurations with the $\nu\bar{\nu}$ pair originating from a Z boson are preferred, the recoil mass of the single electron candidate is required to be greater than 95 GeV.

Independent tests reveal a trigger efficiency of 90% for this channel, the selection efficiency is around 73% using EXCALIBUR. The energy spectrum of the selected candidate events is presented in Figure 3. The numbers of observed and expected events as well as the prediction for the signal and the selection efficiency are summarized in Table 1.

3.2.2 Single Muon Final States

For the single muon final states, the muon energy, measured in in the Muon Chambers and in the central tracker, is required to exceed 20 GeV. The fiducial volume for this analysis is defined to be $|\cos\theta_\mu| < 0.85$. This latter requirement reflect significant decrease of the trigger efficiency for single muons in the angular region $|\cos\theta_\mu| > 0.85$. The trigger efficiency is around 95%, selection efficiencies range between 52.1 % and 53.6%. The energy spectrum of the selected single muon candidates is presented in Figure 4. Table 1 summarizes the observed and expected number of events at each centre-of-mass energy.

3.2.3 Single Tau Final States

For the single tau final states the calorimetric energy associated with the τ jet must exceed 15 GeV. The number of tracks reconstructed in the central tracking system must be either 1 or 3. The mass of the τ-jet candidate must not exceed 4 GeV and its opening angle is required to be less than 15°. The signal efficiency is estimated to be 30.3% to 31.3% using EXCALIBUR, slightly depending on the centre-of-mass energy. The trigger efficiency was studied and found to be in excess of 98%. The energy spectrum of selected single tau candidates is presented in Figure 5, numbers of observed and expected events are given in Table 1.

The total cross section for the leptonic decays of single W production is determined by a binned log-likelihood fit to the lepton energy spectrum as it is shown in Figure 6. The following table summarizes the measurements at the four centre-of-mass energies. A breakdown of all lepton candidates is illustrated in Figure 7.

$\sqrt{s}$ [GeV]	$\sigma_{\ell\nu} \pm$ (stat.) $\pm$ (syst.) [pb]	$\sigma_{\ell\nu}^{\mathrm{Ex}}$ [pb]	$\sigma_{\ell\nu}^{\mathrm{Gr}}$ [pb]
192	$0.19 \; ^{+0.17}_{-0.13} \; \pm 0.02$	0.195	0.182
196	$0.23 \; ^{+0.10}_{-0.08} \; \pm 0.02$	0.213	0.196
200	$0.27 \; ^{+0.11}_{-0.09} \; \pm 0.02$	0.229	0.209
202	$0.25 \; ^{+0.16}_{-0.12} \; \pm 0.02$	0.232	0.215

4 Systematic Errors

The dominant systematic error arises from the uncertainty in the signal modelling. It is found to be approximately 4% in the lepton channels comparing the signal efficiencies estimated using the two Monte Carlo generators, GRC4F and EXCALIBUR. The systematic error arising from the selection criteria is less than 1.5%, estimated by a variation of the different cuts.

In case of the hadronic decay of the single W, 2% difference in signal efficiencies must be taken into account. Two neural networks are trained using either EXCALIBUR or GRC4F Monte Carlo. Then, the cross-section from a fit to each neural network is determined, comparing the response of the EXCALIBUR and GRC4F signal description. This yields a maximal difference of 2.5% which must be taken into account as an additional systematic uncertainty.

Moreover, the parameters describing the neural network structure are varied and the analysis is repeated to allow an estimation of the uncertainty due to the choice of the network. This systematic error is found to be approximately 3%. Compared to this systematic uncertainty, smearing the kinematic variables that are fed into the network within the experimental resolution has only negligible impact on the result.

The error due to the Monte Carlo signal statistics ranges from 1% to 3% depending on the decay channel. The systematic error on the expected number of background events is essentially due to the limited Monte Carlo statistics, with smaller contributions from the uncertainties on the cross sections and the selection efficiency for the background processes. The overall error on the total number of background events ranges from 3% to 4% of the number of expected background events in the individual channels. These uncertainties are uncorrelated among individual channels and different centre-of-mass energies and have negligible impact on the final results.

Cross Sections are determined by binned log-likelihood fits assuming Poisson statistics. A possible source of uncertainty may arise due to the choice of binning used in the fit. Varying the number of bins, this contribution to the systematic uncertainty is found to be less than 1.8% for all channels.

5 Results

5.1 Total Cross Section

The total cross-section of all signal processes is determined from a binned likelihood fit to the distributions of the neural network output presented in Figure 2 and the lepton energy spectra shown in Figures 3-6. The background shapes and normalisations are fixed to the Monte Carlo prediction. The fitted signal cross-section, $\sigma(\mathrm{e^+e^-} \rightarrow \mathrm{e}\nu_\mathrm{e}\mathrm{W})$, corresponds to that of the process $\mathrm{e^+e^-} \rightarrow \mathrm{e}\nu_\mathrm{e}\mathrm{f}\,\bar{\mathrm{f}}'$, where $\mathrm{f}\,\bar{\mathrm{f}}'$ denotes a sum of all $\ell\nu_\ell$ and $q\bar{q}'$ final states satisfying the phase space conditions (2). The relative contribution of the non-resonant $\mathrm{e}\nu_\mathrm{e}\mathrm{f}\,\bar{\mathrm{f}}'$ final states to the signal is fixed to the EXCALIBUR prediction. The total single W boson cross-sections at the four centre-of-mass energies are listed in the following table:

$\sqrt{s}$ [GeV]	$\sigma_{\mathrm{e}\nu\mathrm{W}} \pm$ (stat.) $\pm$ (syst.) [pb]	$\sigma^{\mathrm{Ex}}_{\mathrm{e}\nu\mathrm{W}}$ [pb]	$\sigma^{\mathrm{Gr}}_{\mathrm{e}\nu\mathrm{W}}$ [pb]
192	$0.82\ ^{+0.37}_{-0.32}\ \pm0.07$	0.593	0.588
196	$0.76\ ^{+0.21}_{-0.19}\ \pm0.07$	0.652	0.631
200	$0.61\ ^{+0.20}_{-0.18}\ \pm0.05$	0.689	0.674
202	$1.07\ ^{+0.35}_{-0.31}\ \pm0.10$	0.706	0.695

The measured cross-section values are consistent with the Standard Model predictions calculated with GRC4F and EXCALIBUR. The dependence of the cross section on the centre-of-mass energy agrees well with the Standard Model predictions as shown in Figure 8.

5.2 WWγ Gauge Couplings

The electromagnetic gauge couplings κ_γ and λ_γ describing the WWγ vertex are determined from a binned maximum-likelihood fit similar to the one used for the cross section determination. In the fit each Monte Carlo event is assigned a weight that depends on the generated event kinematics and the values of the gauge couplings κ_γ and λ_γ. The dependence of the background processes on the gauge couplings is also taken into account. The weight is calculated using the matrix element as implemented in EXCALIBUR, imposing constraints on the other triple gauge boson couplings g_1^Z, κ_Z and λ_Z arising from the $SU(2) \times U(1)$ gauge invariance: $\kappa_\mathrm{Z} = g_1^\mathrm{Z} - \tan^2\theta_\mathrm{w} \cdot (\kappa_\gamma - 1)$ and $\lambda_\mathrm{Z} = \lambda_\gamma$. These constraints affect only the background contributions, as the signal process depends on λ_γ and κ_γ only. The general analysis of g_1^Z, λ_γ and κ_γ can only be done with full consideration of the W-pair production [21]. In the present analysis we assume that the weak charge of the W bosons is one, $g_1^\mathrm{Z} = 1$, and focus on the electromagnetic properties of W bosons.

Systematic errors are studied in detail at $\sqrt{s} = 189$ GeV and are taken as estimates for the preliminary results presented here. Because of the small differences between the cross sections predicted by GRC4F and EXCALIBUR, the agreement between the two generators for various anomalous couplings is checked. The test reveals no coupling-dependence as regards the ratio of the two theoretical predictions. The dominant systematic error arises from the difference in the signal efficiency estimated using the two Monte Carlo generators. This uncertainty is found to be approximately 5% and 6% on κ_γ and λ_γ, respectively. To test the dependence of the coupling determination on the total cross section for single W boson production, the likelihood fit is repeated varying the cross section by $\pm 7\%$. The corresponding systematic error is 4% for κ_γ and 2% for λ_γ. In addition, the cross section of the background contributions coming from $\mathrm{W^+W^-}$ and ZZ production are varied to allow an estimation of the systematic uncertainty due to these predictions: the $\mathrm{W^+W^-}$ cross section is varied by $\pm 2.5\%$ which corresponds to the statistical accuracy of this measurement at 189 GeV. Comparing the prediction by EXCALIBUR for ZZ production with the PYTHIA description reveals a difference of 17% after the selection. Although EXCALIBUR is preferred to PYTHIA in the analysis, half of this difference is used as a variation of the ZZ cross section. The influence of these uncertainties on the coupling determination is found to be less than 2%. The estimated systematic error is assumed to be Gaussian and fully correlated between individual selection channels. The systematic uncertainty in the cross section determination is taken into account by convolution of the likelihood function with this Gaussian in the fit.

For the couplings fits we combined the single W data at centre-of-mass energies $\sqrt{s} = 192\ \mathrm{GeV} - 202\ \mathrm{GeV}$ with the single W data selected at energies up to 189 GeV. As it is illustrated in Figure 9, single W boson production is particularly sensitive to the gauge coupling κ_γ. Thus, the coupling is determined in a fit fixing $\lambda_\gamma = 0$:

$$\kappa_\gamma \quad = \quad +1.10^{+0.10}_{-0.10} \pm 0.08\,. \tag{3}$$

Fixing $\kappa_\gamma = 1$ and performing a fit for λ_γ yields

$$\lambda_\gamma \quad = \quad -0.20^{+0.59}_{-0.16} \pm 0.11\,. \tag{4}$$

Varying both couplings λ_γ and κ_γ freely in the fit yields:

$$\kappa_\gamma \quad = \quad +1.10^{+0.10}_{-0.11} \pm 0.08 \tag{5}$$
$$\lambda_\gamma \quad = \quad -0.10^{+0.41}_{-0.22} \pm 0.11\,, \tag{6}$$

with a correlation of 31.6%. This result is consistent with the absence of anomalous contribution to WWγ couplings. The limits on κ_γ and λ_γ at 95% confidence level are:

$$0.87 \ < \ \kappa_\gamma \ < \ 1.30 \quad \text{for} \quad \lambda_\gamma = 0 \tag{7}$$
$$-0.49 \ < \ \lambda_\gamma \ < \ 0.53 \quad \text{for} \quad \kappa_\gamma = 1\,. \tag{8}$$

The 68% and 95% confidence level contours are shown in Figure 10. These results represent a considerable improvement in the accuracy on the triple gauge boson couplings λ_γ and κ_γ compared to our previous measurement using single W boson production as illustrated in Figure 11. These results are complementary and among the most stringent measurements compared to those determined from $\mathrm{W^+W^-}$ production [21, 22] or at the $\mathrm{p\overline{p}}$ collider Tevatron [23, 24], in particular as regards κ_γ.

Acknowledgements

We wish to express our gratitude to the CERN accelerator divisions for the excellent performance of the LEP machine. We acknowledge the efforts of the engineers, technicians and support staff who have participated in the construction and maintenance of this experiment.

References

[1] S. L. Glashow, Nucl. Phys. **22** (1961) 579;
S. Weinberg, Phys. Rev. Lett. **19** (1967) 1264;
A. Salam, "Elementary Particle Theory", Ed. N.Svartholm, Stockholm, "Almquist and Wiksell", (1968), 367.

[2] M. Acciarri *et al.*, L3 Collaboration, Phys. Lett. **B403** (1997) 168.

[3] M. Acciarri *et al.*, L3 Collaboration, Phys. Lett. **B436** (1998) 417.

[4] R. Barate *et al.*, ALEPH Collaboration, Phys. Lett. **B462** (1999) 389.

[5] T. Tsukamoto and Y. Kurihara, Phys. Lett. **B389** (1996), 162.

[6] J. Fujimoto *et al.*, Comp. Phys. Comm. **100** (1997) 128.

[7] F. A. Berends, R. Pittau and R. Kleiss, Comp. Phys. Comm. **85** (1995) 437.

[8] S. Jadach, B.F.L. Ward and Z. Wąs, Comp. Phys. Comm. **79** (1994) 503.

[9] M. Skrzypek *et al.*, Comp. Phys. Comm. **94** (1996) 216; M. Skrzypek *et al.*, Phys. Lett. **B372** (1996) 289.

[10] D. Karlen, Nucl. Phys. **B289** (1987) 23.

[11] J. H. Field, Phys. Lett. **B323** (1994) 432; J. H. Field and T. Riemann, Comp. Phys. Comm. **94** (1996) 53.

[12] S. Jadach, W. Placzek und B.F.L. Ward, Phys. Lett. **B390** (1997) 298.

[13] T. Sjöstrand, CERN-TH/7112/93 (1993), revised August 1995; T. Sjöstrand, Comp. Phys. Comm. **82** (1994) 74.

[14] S. Jadach, B. F. L. Ward and Z. Wąs, CERN-TH/235/99 (1999).

[15] R. Engel, Z.Phys. **C66** (1995) 203; R. Engel, J. Ranft and S. Roesler, Phys. Rev. **D52** (1995) 1459.

[16] R. Brun *et al.*, preprint CERN DD/EE/84-1 (Revised 1987).

[17] H. Fesefeldt, RWTH Aachen Report PITHA 85/02 (1985).

[18] S. Catani *et al.*, Phys. Lett. **B269** (1991) 432;
S. Bethke *et al.*, Nucl. Phys. **B370** (1992) 310.

[19] L. Lönnblad, C. Peterson and T. Rögnvaldsson, Nucl. Phys. **B349** (1991) 675;
C. Peterson *et al.*, Comp. Phys. Comm. **81** (1994) 185.

[20] W. Bartel *et al.*, JADE Collaboration, Z. Phys. **C33** (1986) 23; S. Bethke *et al.*, Phys. Lett. **B213** (1988) 235.

[21] M. Acciari *et al.*, L3 Collaboration, Phys. Lett. **B467** (1999) 171.

[22] R. Barate *et al.*, ALEPH Collaboration, Phys. Lett. **B422** (1998) 369;
K. Ackerstaff *et al.*, OPAL Collaboration, Eur. Phys. J. **C8** (1999) 191;
P. Abreu *et al.*, DELPHI Collaboration, Phys. Lett. **B459** (1999) 382.

[23] B. Abbott *et al.*, DØ Collaboration, Hep-Ex/9912033, submitted to Phys. Rev. D.

[24] F. Abe *et al.*, CDF Collaboration, Phys. Rev. Lett. **75** (1995) 1017.

$\sqrt{s}=192$ GeV	$\mathcal{L}=29.7\,\mathrm{pb}^{-1}$			
Final State	$N^{\mathrm{MC}}_{\mathrm{e}\nu\mathrm{W}}$	Efficiency [%]	N^{MC}	$N_{\mathrm{e}\nu\mathrm{W}}$
$\mathrm{e}^+\nu_\mathrm{e}\mathrm{e}^-\overline{\nu}_\mathrm{e}$	1.34	73.2 ± 1.0	2.41	3
$\mathrm{e}^+\nu_\mathrm{e}\mu^-\overline{\nu}_\mu$	1.12	53.3 ± 0.6	1.78	1
$\mathrm{e}^+\nu_\mathrm{e}\tau^-\overline{\nu}_\tau$	0.48	30.5 ± 0.6	0.83	1
$\mathrm{e}^+\nu_\mathrm{e}\ell^-\overline{\nu}_\ell$	2.94	51.6 ± 0.8	5.02	5
$\mathrm{e}^+\nu_\mathrm{e}\mathrm{q}\,\bar{\mathrm{q}}'$	5.76	47.4 ± 0.5	26.41	26

$\sqrt{s}=196$ GeV	$\mathcal{L}=83.7\,\mathrm{pb}^{-1}$			
Final State	$N^{\mathrm{MC}}_{\mathrm{e}\nu\mathrm{W}}$	Efficiency [%]	N^{MC}	$N_{\mathrm{e}\nu\mathrm{W}}$
$\mathrm{e}^+\nu_\mathrm{e}\mathrm{e}^-\overline{\nu}_\mathrm{e}$	4.17	74.0 ± 1.0	7.92	9
$\mathrm{e}^+\nu_\mathrm{e}\mu^-\overline{\nu}_\mu$	3.46	53.6 ± 0.6	4.33	4
$\mathrm{e}^+\nu_\mathrm{e}\tau^-\overline{\nu}_\tau$	1.44	30.3 ± 0.6	2.59	2
$\mathrm{e}^+\nu_\mathrm{e}\ell^-\overline{\nu}_\ell$	9.07	51.7 ± 0.8	14.84	15
$\mathrm{e}^+\nu_\mathrm{e}\mathrm{q}\,\bar{\mathrm{q}}'$	17.64	48.6 ± 0.5	79.69	92

$\sqrt{s}=200$ GeV	$\mathcal{L}=82.8\,\mathrm{pb}^{-1}$			
Final State	$N^{\mathrm{MC}}_{\mathrm{e}\nu\mathrm{W}}$	Efficiency [%]	N^{MC}	$N_{\mathrm{e}\nu\mathrm{W}}$
$\mathrm{e}^+\nu_\mathrm{e}\mathrm{e}^-\overline{\nu}_\mathrm{e}$	4.33	71.9 ± 1.4	7.83	13
$\mathrm{e}^+\nu_\mathrm{e}\mu^-\overline{\nu}_\mu$	3.59	52.1 ± 0.6	4.94	3
$\mathrm{e}^+\nu_\mathrm{e}\tau^-\overline{\nu}_\tau$	1.52	30.1 ± 0.6	2.43	2
$\mathrm{e}^+\nu_\mathrm{e}\ell^-\overline{\nu}_\ell$	9.44	50.7 ± 1.0	15.20	18
$\mathrm{e}^+\nu_\mathrm{e}\mathrm{q}\,\bar{\mathrm{q}}'$	19.28	49.6 ± 0.6	82.42	77

$\sqrt{s}=202$ GeV	$\mathcal{L}=37.0\,\mathrm{pb}^{-1}$			
Final State	$N^{\mathrm{MC}}_{\mathrm{e}\nu\mathrm{W}}$	Efficiency [%]	N^{MC}	$N_{\mathrm{e}\nu\mathrm{W}}$
$\mathrm{e}^+\nu_\mathrm{e}\mathrm{e}^-\overline{\nu}_\mathrm{e}$	2.02	75.0 ± 1.4	3.57	6
$\mathrm{e}^+\nu_\mathrm{e}\mu^-\overline{\nu}_\mu$	1.70	53.6 ± 0.8	2.29	1
$\mathrm{e}^+\nu_\mathrm{e}\tau^-\overline{\nu}_\tau$	0.73	31.3 ± 0.8	1.16	1
$\mathrm{e}^+\nu_\mathrm{e}\ell^-\overline{\nu}_\ell$	4.45	52.3 ± 1.1	7.02	8
$\mathrm{e}^+\nu_\mathrm{e}\mathrm{q}\,\bar{\mathrm{q}}'$	9.11	51.5 ± 0.6	36.87	46

Table 1: The number of selected candidates for single W boson production, $N_{\mathrm{e}\nu\mathrm{W}}$, compared to the total number of expected events, N^{MC}, for each decay channel of the W boson. In addition, the expected number of signal events, $N^{\mathrm{MC}}_{\mathrm{e}\nu\mathrm{W}}$, and the signal efficiency of the selection in each channel are given, using the EXCALIBUR Monte Carlo.

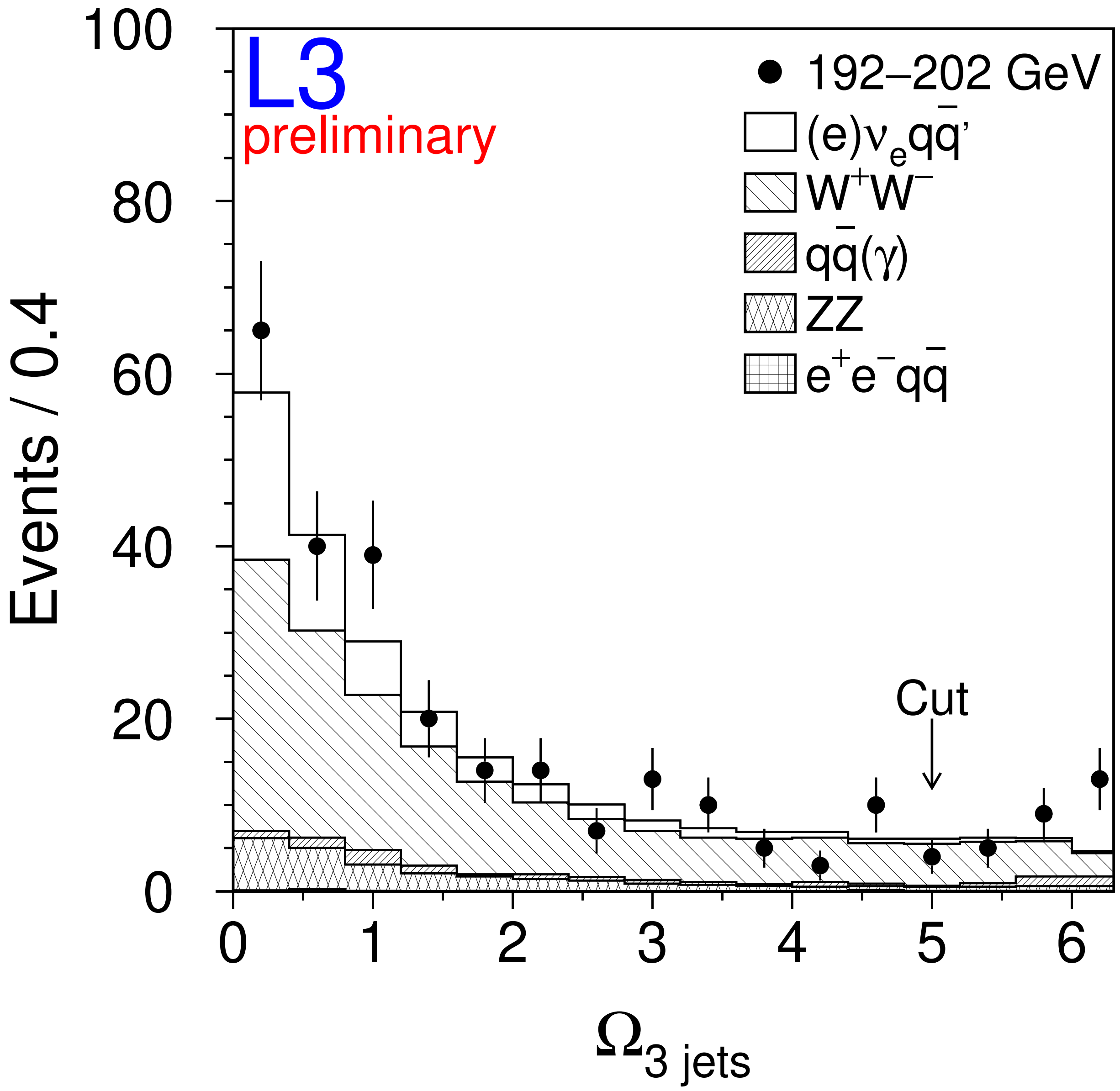

Figure 1: Distribution of the 3-jet opening angle Ω for the selected hadronic events at $\sqrt{s}$ = 192 GeV − 202 GeV. The dots are data, the hatched histograms represent the backgrounds and the open histograms show the expected signal from $e^+\nu_e q\,\bar{q}'$ final states.

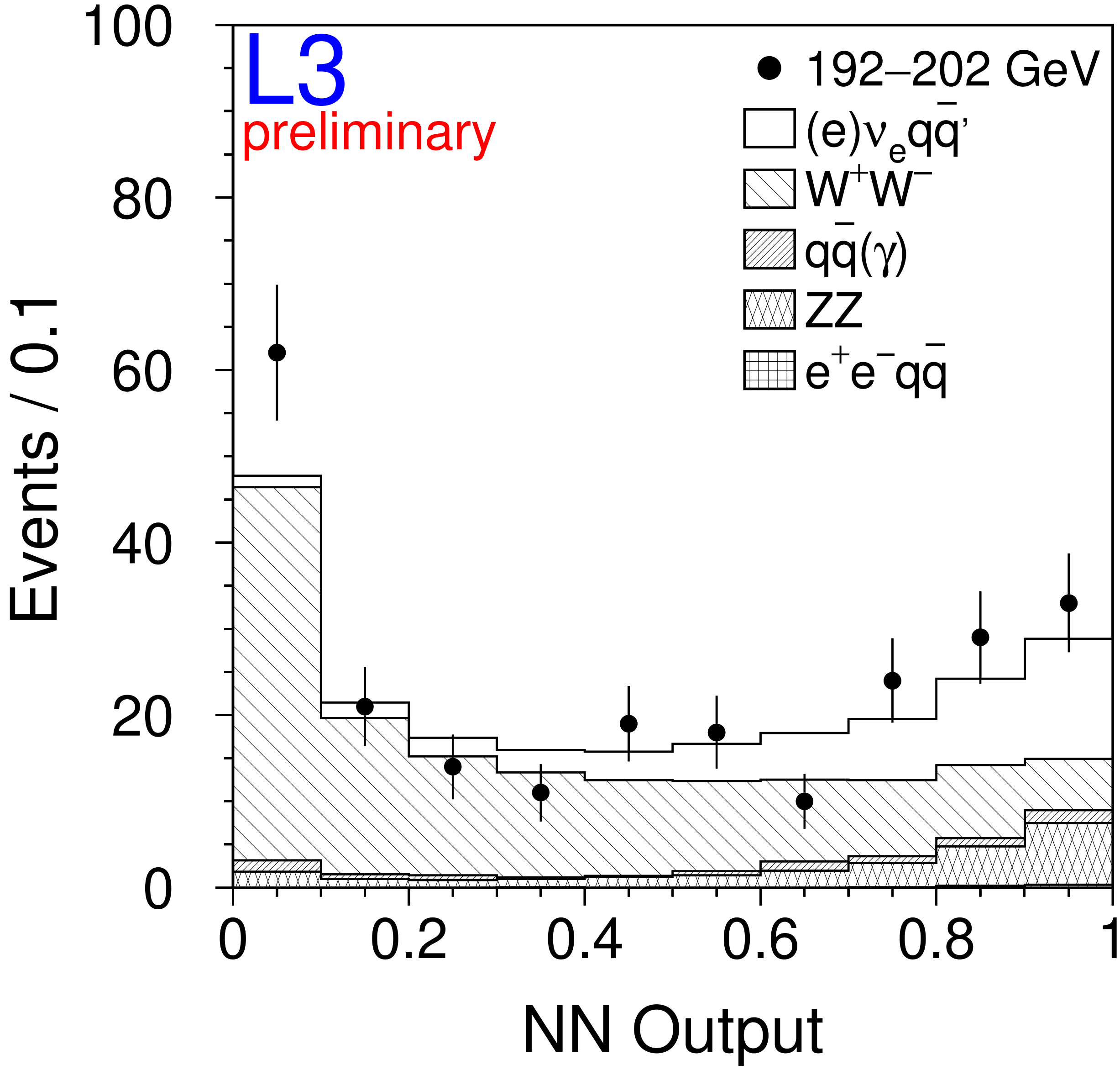

Figure 2: Distribution of the neural network output used in the selection of hadronic decays of single W bosons. The data collected at centre-of-mass energies between $\sqrt{s} = 192$ GeV and $\sqrt{s} = 202$ GeV are shown, together with the background contributions and the expected signal, represented by the hatched and open histograms, respectively.

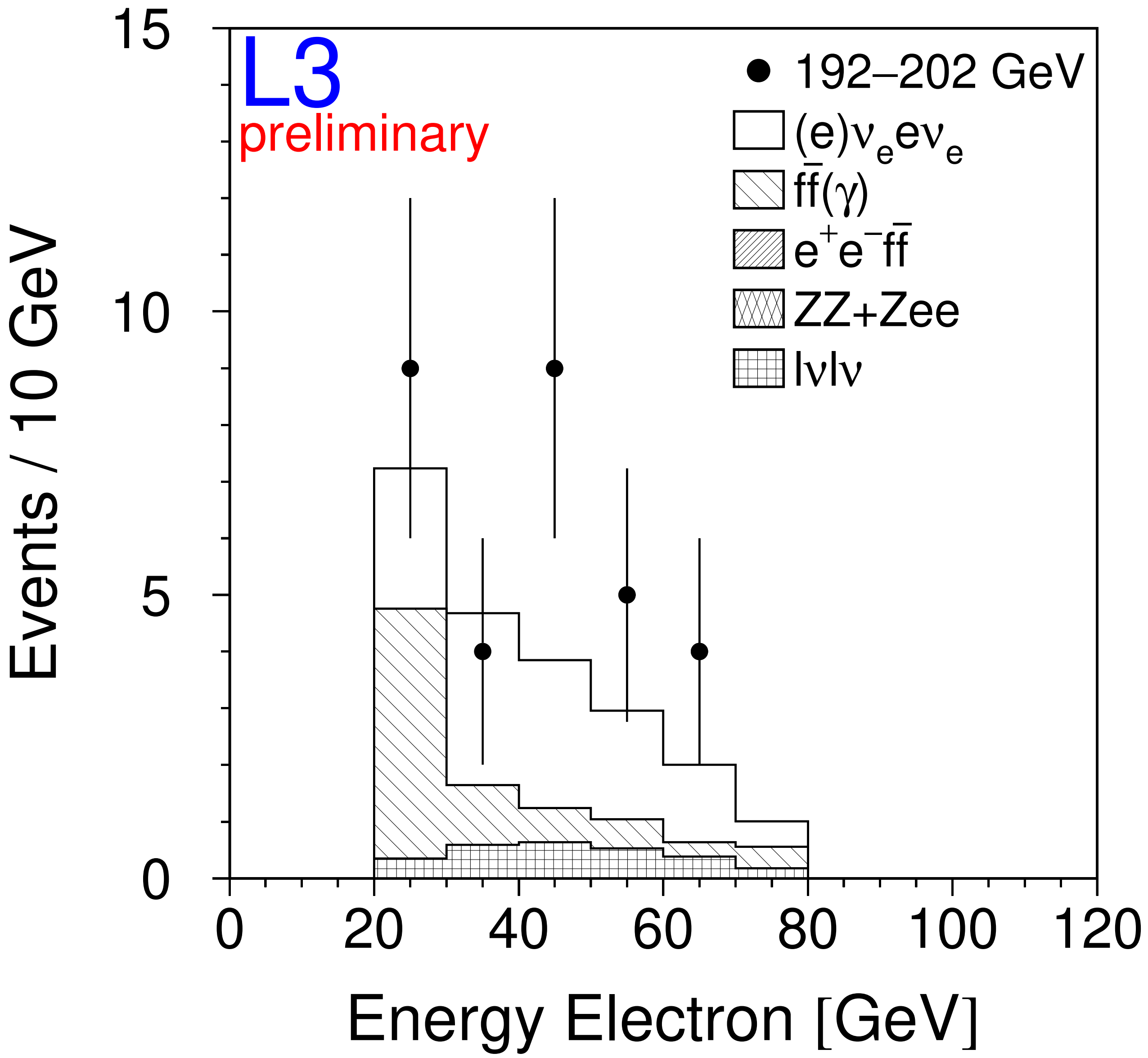

Figure 3: The energy spectra of the selected single electron candidates. The dots are data, the hatched histogram corresponds to the background contribution. The open histogram show the expected signal from $e^+\nu_e e^-\bar{\nu}_e$ final states.

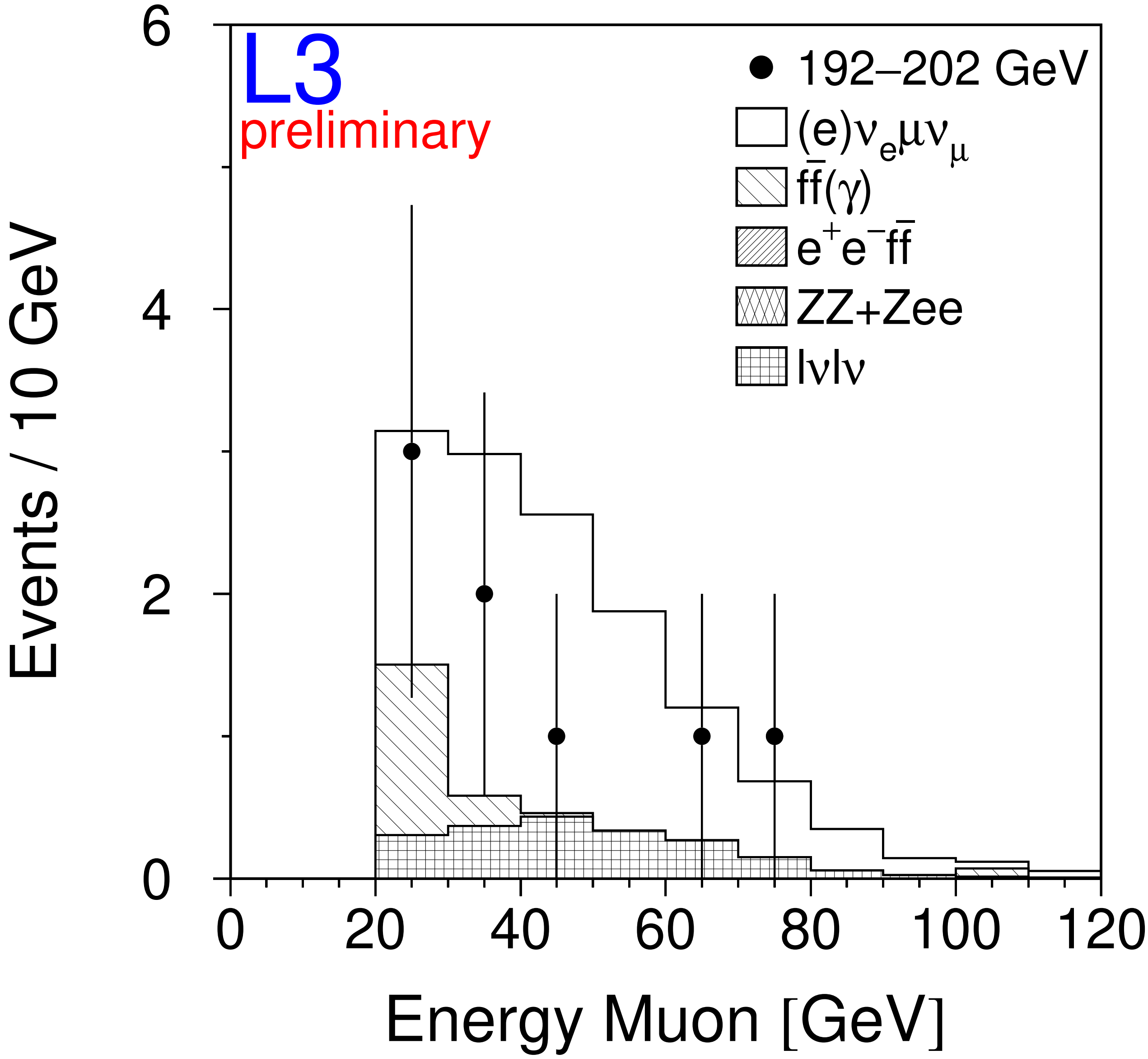

Figure 4: The energy spectrum of the selected single muon candidates. The dots are data, the hatched histogram corresponds to the background contribution. The open histogram show the expected signal from $e\nu_e\mu\nu_\mu$ final states.

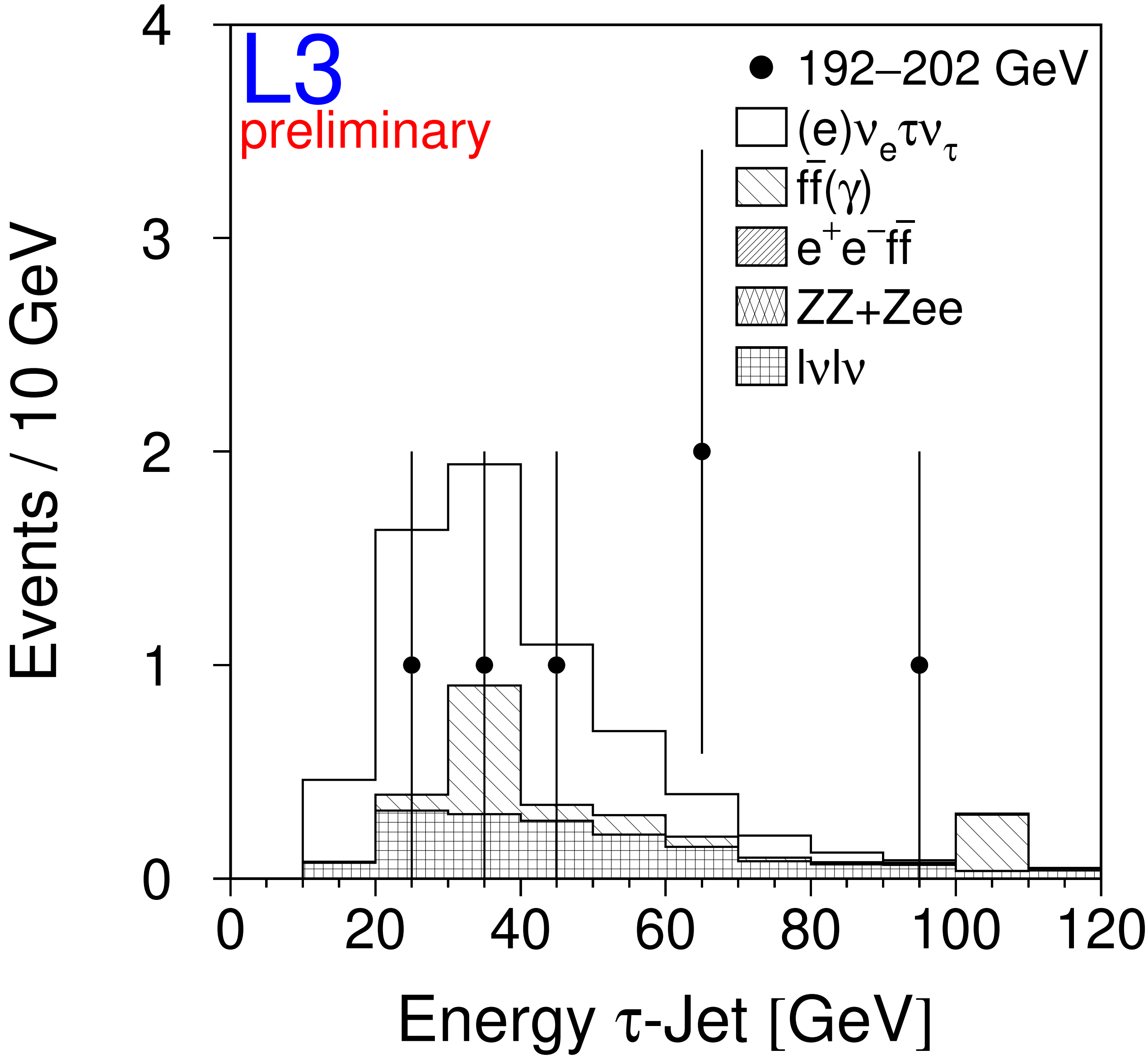

Figure 5: The energy spectra of the selected single tau candidates. The dots are data, the hatched histogram corresponds to the background contribution. The open histogram show the expected signal from $e\nu_e\tau\nu_\tau$ final states.

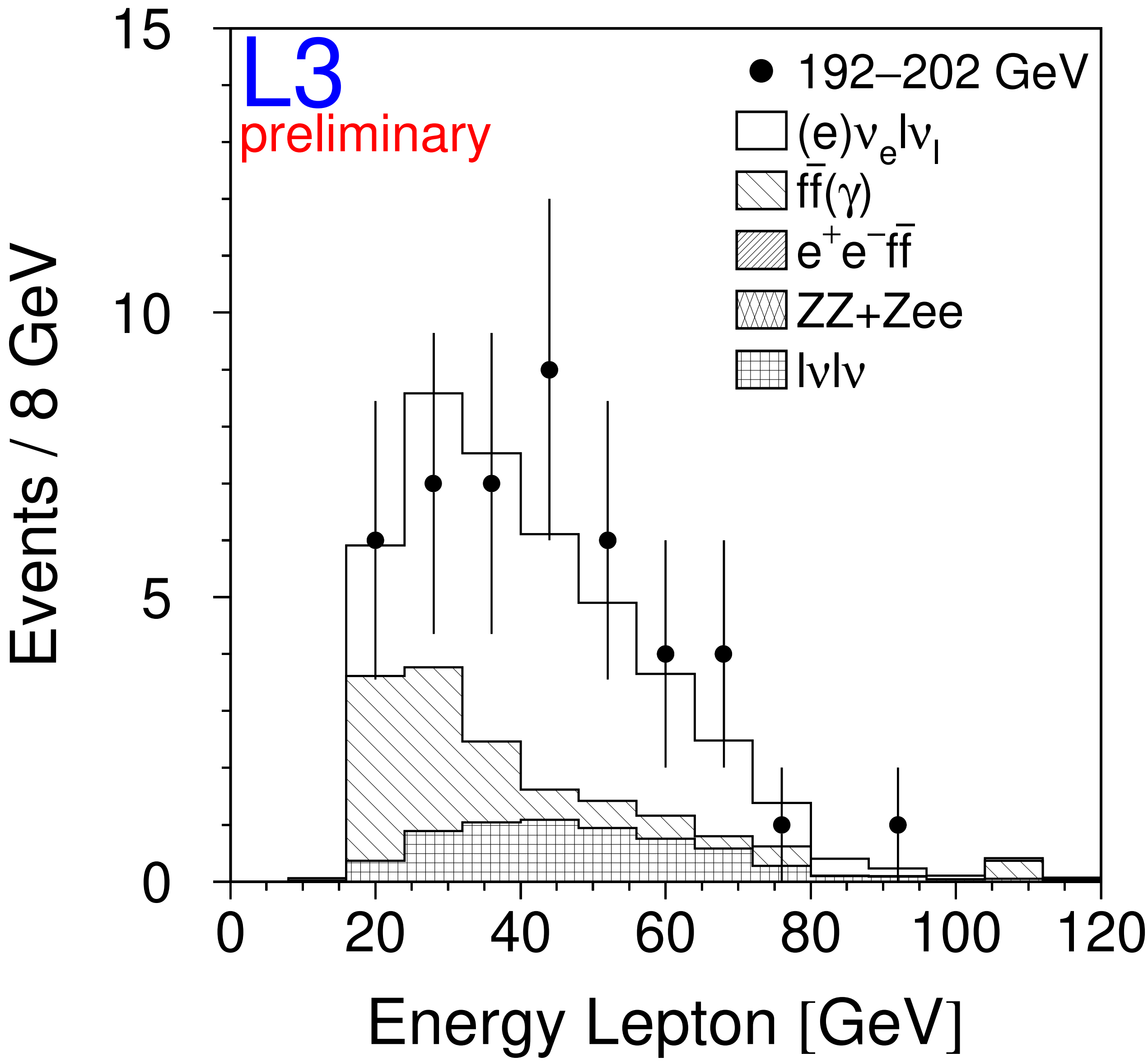

Figure 6: The energy spectrum of the lepton candidates, selected as electrons, muons or hadronic τ-jets. The dots are data, the hatched histogram corresponds to the background contribution. The open histogram show the expected signal from $\mathrm{e}\nu_\mathrm{e}\ell\nu_\ell$ final states.

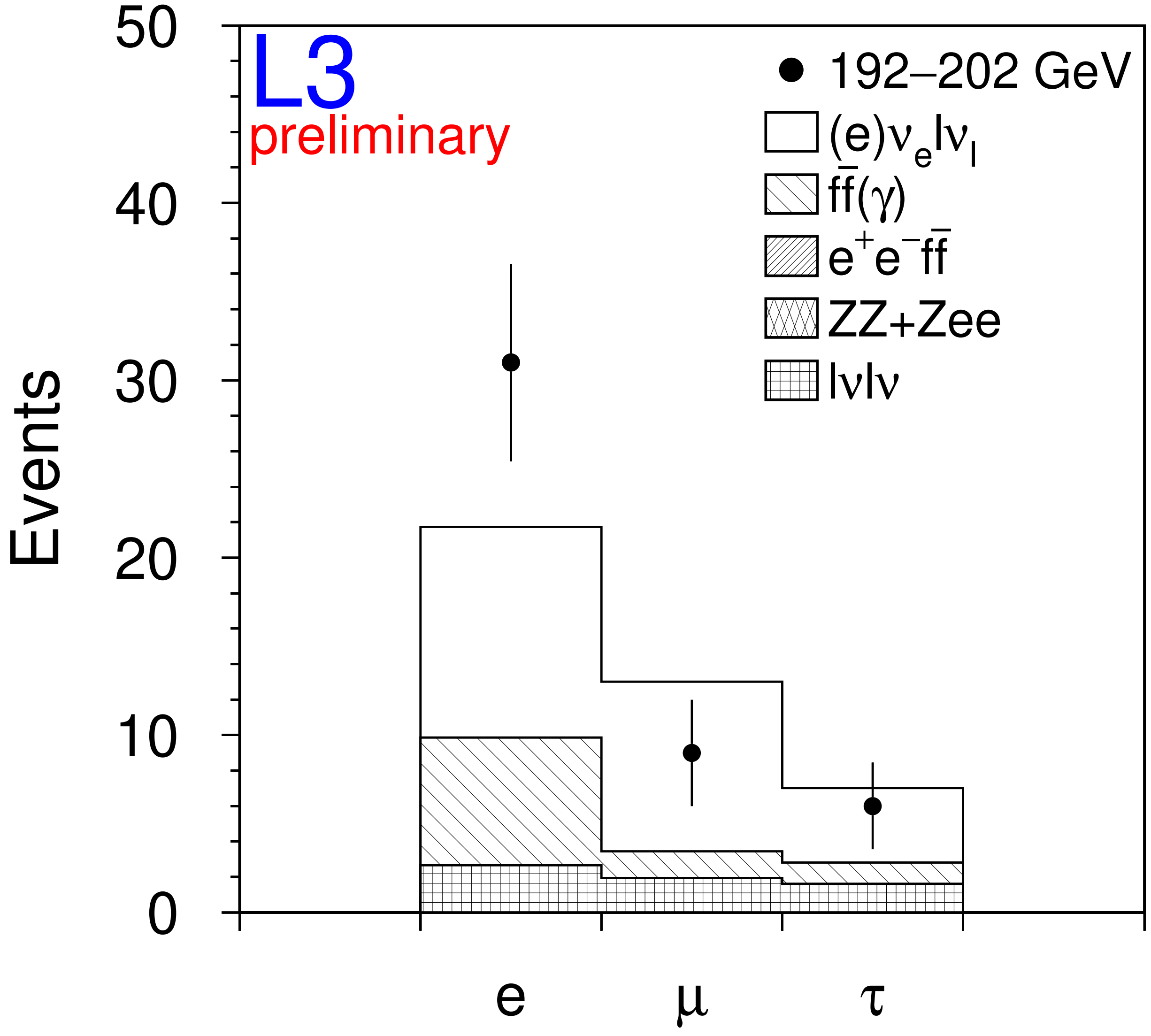

Figure 7: Breakdown of the single lepton candidates selected at centre-of-mass energies between $\sqrt{s} = 192$ GeV and $\sqrt{s} = 202$ GeV.

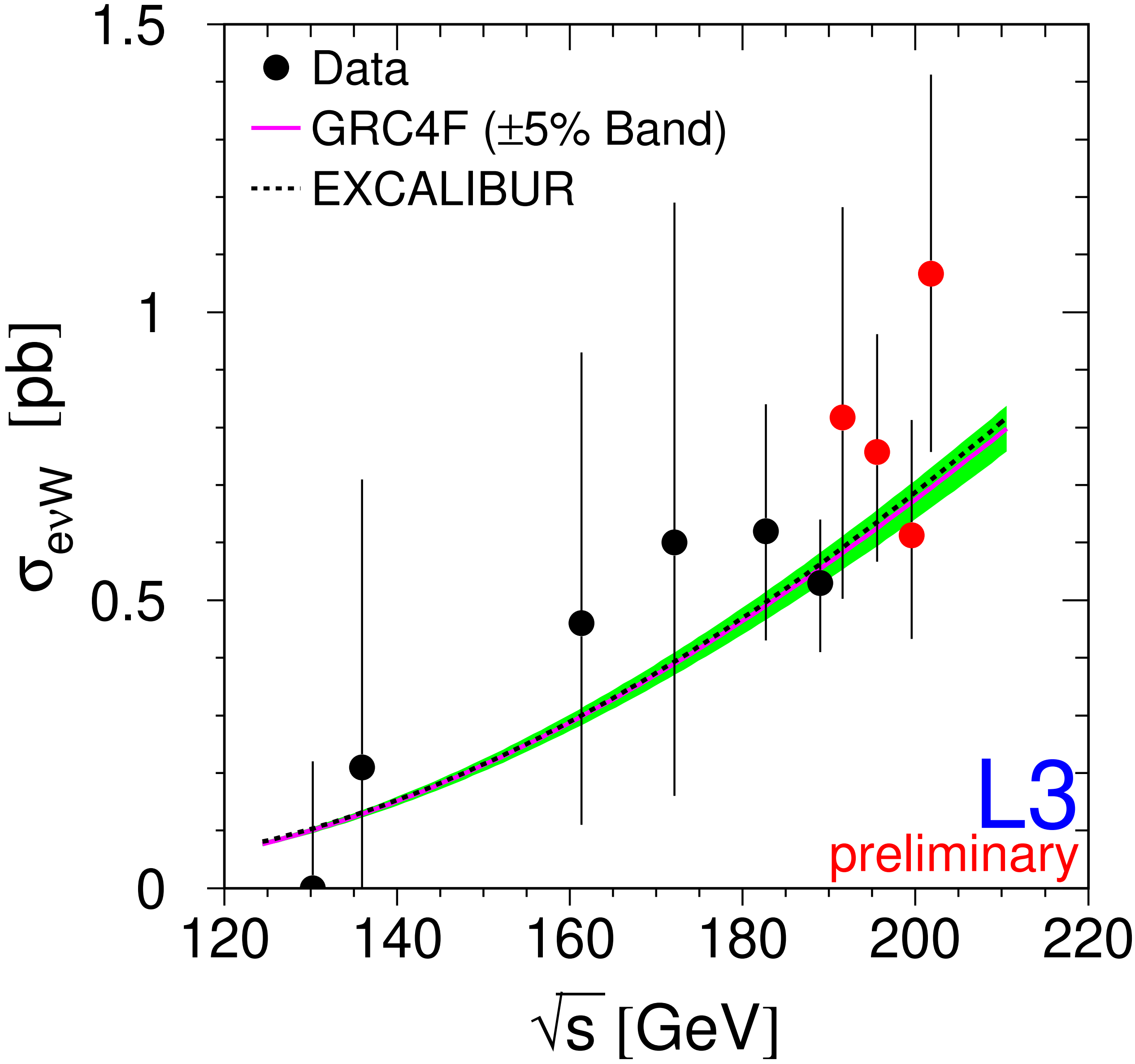

Figure 8: The measured cross section of single W production as a function of the centre-of-mass energy. Each point represents the most likely cross section value at a given centre-of-mass energy. The error bars correspond to the 68% confidence intervals obtained from the cross section fit. The solid and dashed lines show predictions of the GRC4F and EXCALIBUR Monte Carlo programs. A $\pm 5\%$ band is added to illustrate the theoretical uncertainty.

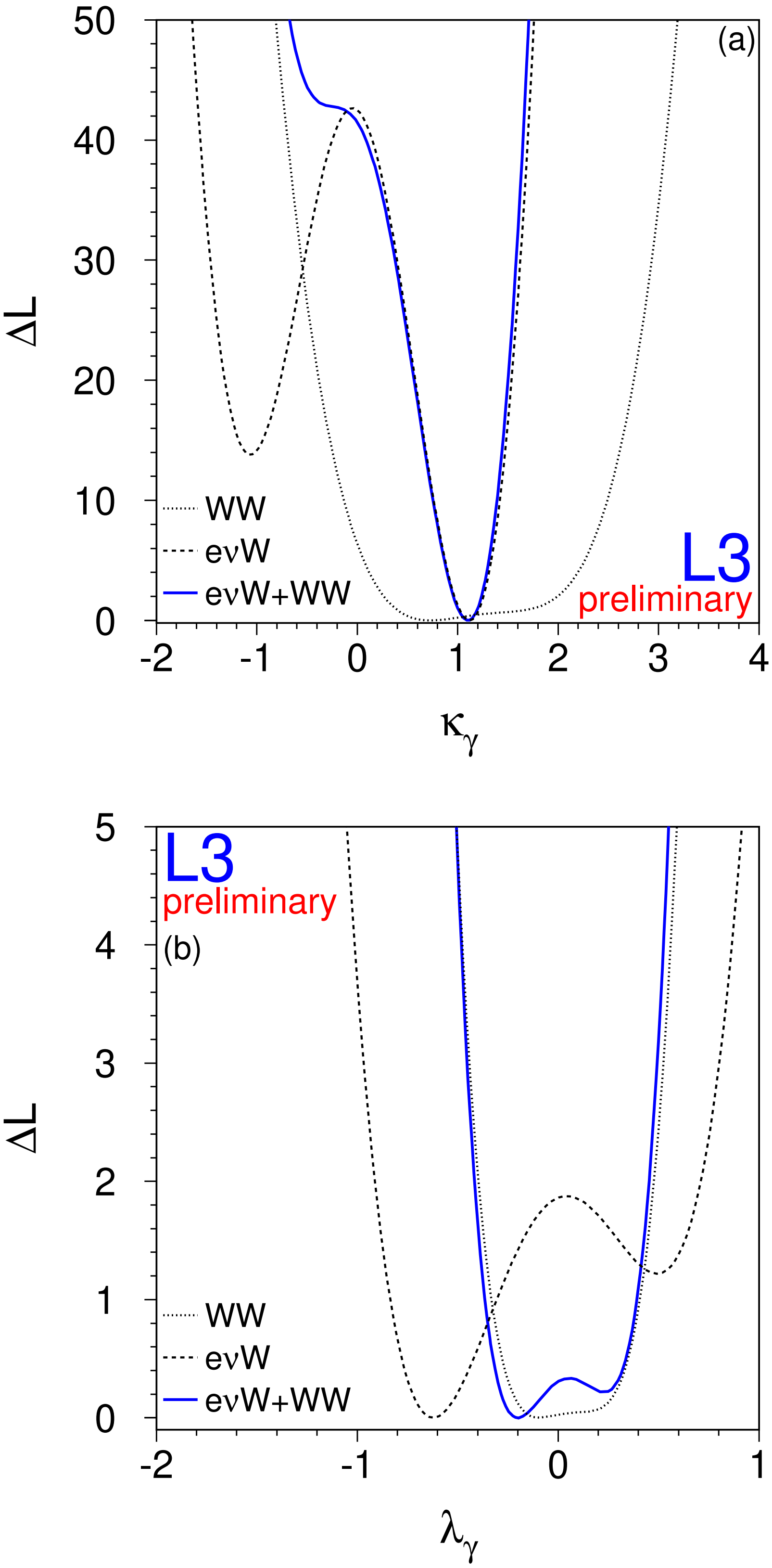

Figure 9: The dependence of the log-likelihood function, $\Delta\log(\mathrm{L})$, on the γWW gauge couplings (a) κ_γ and (b) λ_γ. The other coupling is fixed to its Standard Model value in the fit. For comparison, the individual contributions of the signal and the WW background are also shown.

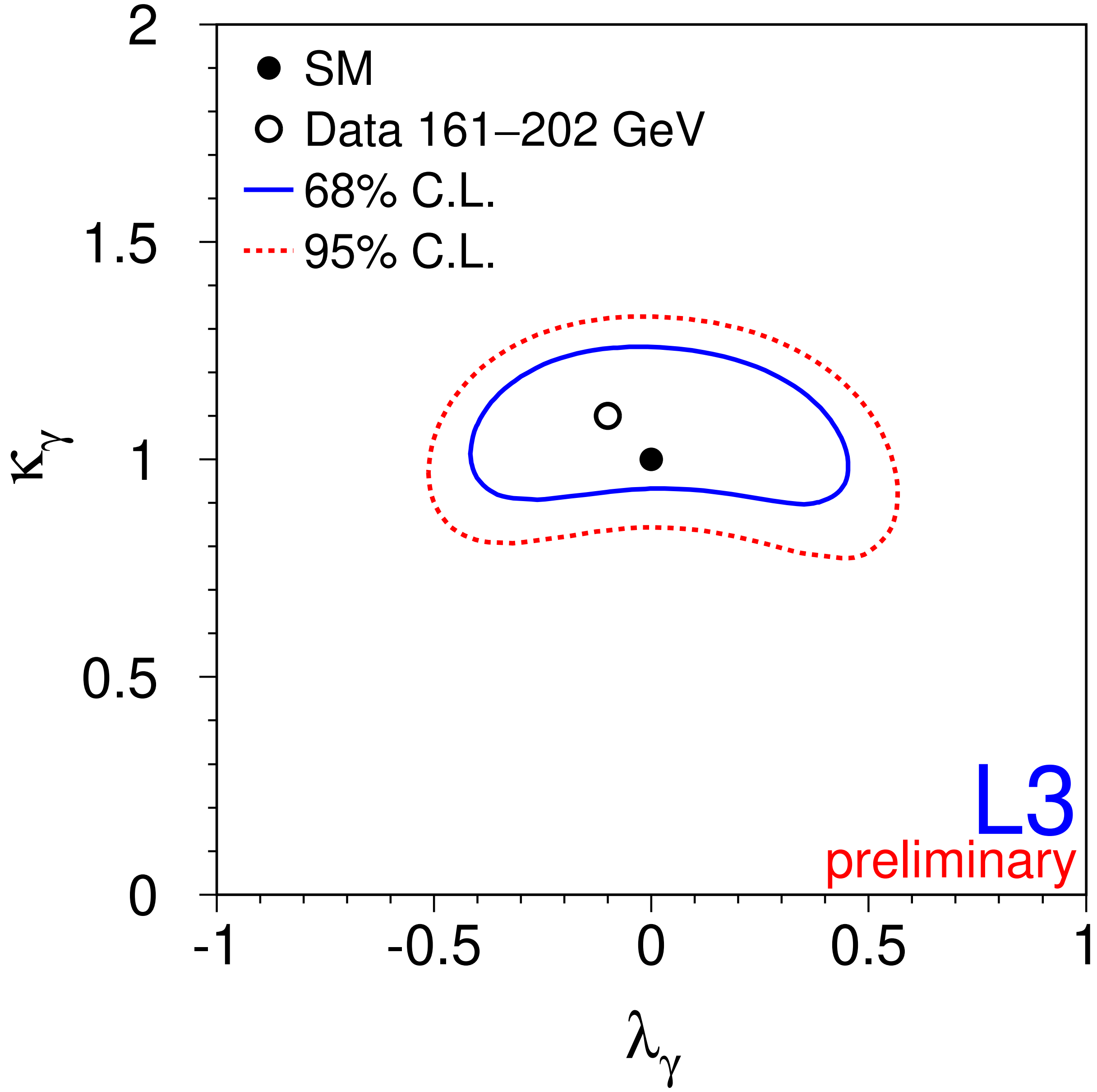

Figure 10: The contours corresponding to 68% and 95% confidence level exclusion limits in the $\kappa_\gamma - \lambda_\gamma$ plane. The open circle indicates the global minimum from the 2-parameter fit to the data, to be compared with the Standard Model prediction indicated by the dot.

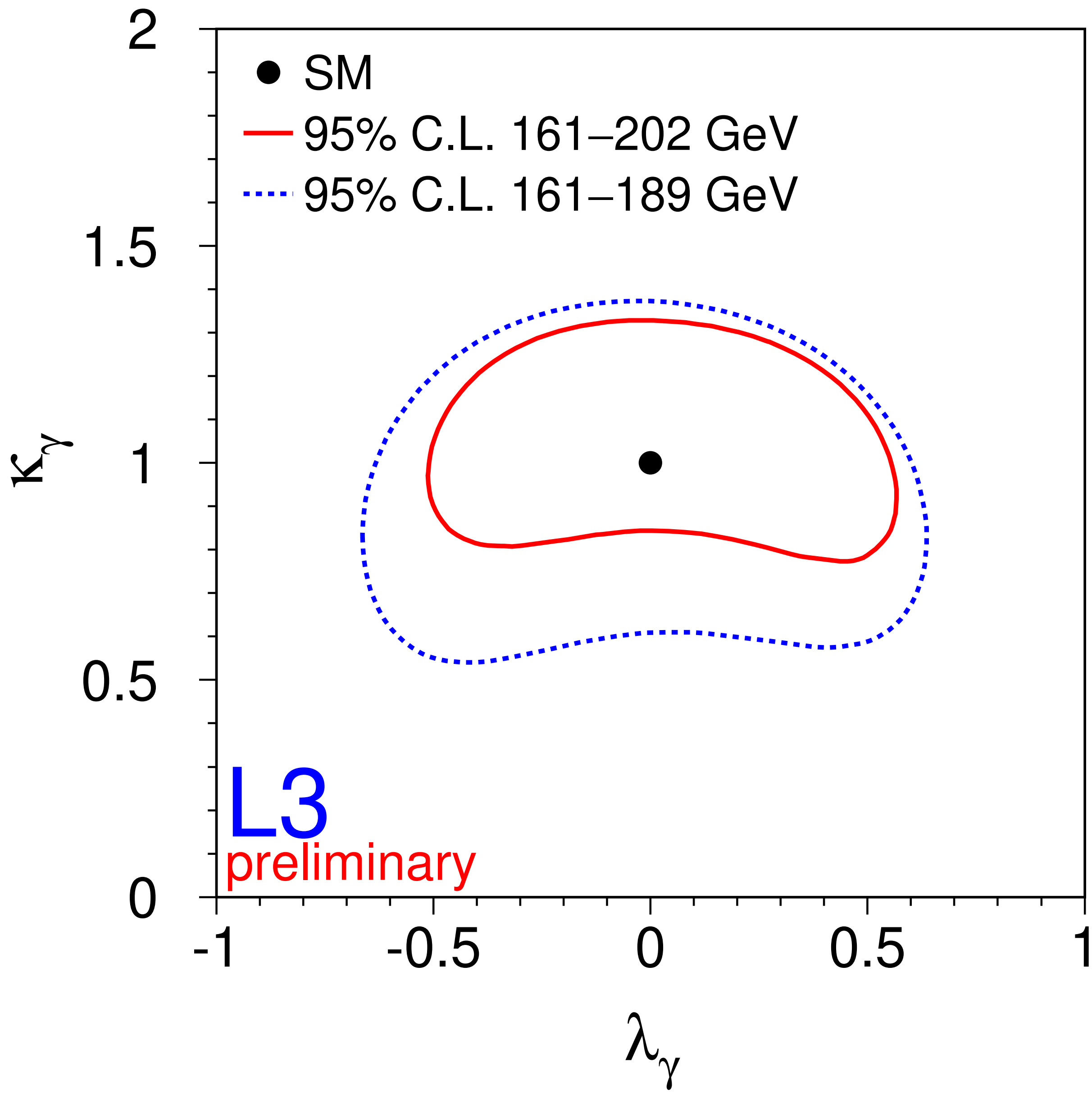

Figure 11: The contours corresponding to 95% confidence level exclusion limits in the $\kappa_\gamma - \lambda_\gamma$ plane, resulting from fits to our previous data up to $\sqrt{s} = 189$ GeV and from fits including the new data up to $\sqrt{s} = 202$ GeV.